

**PHOTOCATALYTIC OXIDATION OF CHITOSAN AND ITS  
DERIVATIVES AND PHENOL BY IMMOBILIZED TiO<sub>2</sub> BILAYER  
ASSEMBLAGE SYSTEMS UNDER VISIBLE LIGHT**

By

**ALI HADI JAWAD AL-TAIE**

**Thesis submitted in fulfillment of the requirements for the degree of Doctor of  
Philosophy**

**2011**

## ACKNOWLEDGEMENTS

First and foremost, I would like to thank Allah for giving me so much blessing to reach this goal. At the same time, I would like to convey my sincere gratitude to my main supervisor, Prof. Dr. Mohd Asri Mohd Nawi for his unlimited guidance, invaluable advice and dedicated support throughout the course of this project. I would also like to thank my co-supervisor, Assoc. Prof. Dr. Wan Saime Wan Ngah for his assistance and support to me throughout the course of my research project.

I would like also to extend my great gratitude to the Malaysia's Ministry of Science and Technology for funding this research project under FRGS: 203/227/PKIMIA/67/027 and IRPA: 305/229/PKIMIA/613402. I am deeply thankful to Universiti Sains Malaysia (USM) for the scholarship under USM Fellowship Scheme. I would also like to gratefully acknowledge all staff members of the School of Chemical Sciences, Institute of Postgraduate Studies (IPS) and School of Biological Sciences. I am deeply grateful to Mr. Aw Yeong, Mr. Ariffin and Mr. Jamal Mohamed for their generous help. I would also like to thank my lab mates in Photocatalysis Laboratory for their sincere assistances. I would also like to express my gratitude to all my faithful friends, especially to Assoc. Prof. Dr. Abbas F. M. Alkarkhi and Dr. Sabah M. Thahab for their moral supports. Finally, to my parents, my brother Dr. Mohamed, my sisters Masar and Esraa for their continued supports during my entire candidature. I wish to thank my wife Roweda and my lovely daughter Rehef for their patience, support and encouragement in all good and hard times.

## TABLE OF CONTENTS

|  | Page     |
|--|----------|
| Acknowledgment   | ii       |
| Table of Contents  | iii      |
| List of Tables   | xi       |
| List of Figures  | xiii     |
| List of Abbreviations and Symbols                            | xxii     |
| Abstrak  | xxiii    |
| Abstract   | xxv      |
| <br>   |          |
| <b>CHAPTER ONE - INTRODUCTION</b>                            | <b>1</b> |
| 1.1 Photocatalysis   | 1        |
| 1.2 Fundamental mechanism of photocatalysis                  | 2        |
| 1.3 TiO <sub>2</sub> as semiconductor photocatalyst          | 4        |
| 1.3.1 General remarks of TiO <sub>2</sub>                    | 4        |
| 1.3.2 Crystallographic structure of TiO <sub>2</sub>         | 6        |
| 1.4 Heterogeneous TiO <sub>2</sub> photocatalysis            | 7        |
| 1.5 Immobilization of TiO <sub>2</sub> photocatalyst         | 14       |
| 1.6 Organic binders  | 17       |
| 1.6.1 Epoxidized natural rubber (ENR)                        | 17       |
| 1.6.2 Phenol-formaldehyde (PF) resin                         | 19       |
| 1.7 Modification of TiO <sub>2</sub> by conventional methods | 20       |
| 1.7.1 Self-sensitization by using colored pollutants         | 21       |
| 1.7.2 Dyes modifying TiO <sub>2</sub>                        | 21       |
| 1.7.3 Doping of TiO <sub>2</sub> with metal ions             | 22       |

|       |  |        |
|-------|--|--------|
| 1.7.4 | Doping of TiO <sub>2</sub> with non-metal atoms                | 23     |
| 1.7.5 | Utilizing different heterojunction systems                     | 24     |
| 1.7.6 | Utilization of thin films                                      | 24     |
| 1.8   | Chitosan (CS) biopolymer                                       | 25     |
| 1.8.1 | Properties of chitosan (CS)                                    | 25     |
| 1.8.2 | Applications of chitosan (CS)                                  | 28     |
| 1.9   | Modifications of chitosan (CS)                                 | 29     |
| 1.9.1 | Physical modification of CS                                    | 29     |
| 1.9.2 | Chemical modification of CS                                    | 30     |
| 1.9.3 | Photo modification of CS                                       | 32     |
| 1.10  | Combining of TiO <sub>2</sub> -CS for water remediation        | 34     |
| 1.11  | Phenol as a model of organic water pollutant                   | 37     |
| 1.12  | Statement of problems  | 38     |
| 1.13  | Research objectives  | 39     |
|       | <br><b>CHAPTER TWO - MATERIALS AND METHODS</b>                 | <br>41 |
| 2.1   | Raw materials and chemicals                                    | 41     |
| 2.2   | Preparation of stock solutions                                 | 41     |
| 2.2.1 | Preparation of phenol and its intermediates                    | 41     |
| 2.2.2 | Preparation of Reactive Red 4 (RR4) dye                        | 42     |
| 2.2.3 | Preparation of chemical oxygen demand (COD) reagent            | 42     |
| 2.3   | Preparation of immobilized CS and its cross-linked derivatives | 43     |
| 2.3.1 | CS solution for immobilization                                 | 43     |
| 2.3.2 | CS solution for chemical cross-linking reaction                | 44     |

|        |  |    |
|--------|--|----|
| 2.3.3  | Immobilization of cross-linked chitosan-glutaraldehyde (CS-GLA) on glass plates  | 44 |
| 2.3.4  | Immobilization of cross-linked chitosan-epichlorohydrine (CS-ECH) on glass plates                                      | 45 |
| 2.4    | Preparation of TiO <sub>2</sub> -ENR <sub>50</sub> -PF dip-coating formulation   | 45 |
| 2.4.1  | Preparation of epoxidized natural rubber <sub>50</sub> (ENR <sub>50</sub> ) solution                                   | 50 |
| 2.4.2  | Determination of the ratio of ENR <sub>50</sub> to toluene   | 46 |
| 2.4.3  | Optimization of PF in TiO <sub>2</sub> -ENR <sub>50</sub> -PF dip-coating formulation                                  | 46 |
| 2.5    | Fabrication of immobilized bilayer TiO <sub>2</sub> /CS, TiO <sub>2</sub> /CS-GLA and TiO <sub>2</sub> /CS-ECH systems | 47 |
| 2.6    | Adhesion of the immobilized TiO <sub>2</sub> layer   | 48 |
| 2.7    | Irradiation reactor set-up   | 49 |
| 2.8    | Adsorption system set-up   | 50 |
| 2.9    | Generation of macro pores on the TiO <sub>2</sub> layer  | 51 |
| 2.9.1  | Diffusion of pollutant molecules   | 52 |
| 2.9.2  | Light and hydroxyl radicals penetration  | 52 |
| 2.10   | Photocatalytic-oxidation of CS and its cross-linked derivatives  | 53 |
| 2.11   | Characterizations  | 54 |
| 2.11.1 | Transmission Electron Microscopy (TEM)   | 54 |
| 2.11.2 | Scanning Electron Microscopy/Energy Dispersive X-ray (SEM / EDX)   | 54 |
| 2.11.3 | Thermal gravimetric analysis (TGA)   | 55 |
| 2.11.4 | Elemental analysis (CHN)   | 55 |
| 2.11.5 | Fourier transform infrared spectroscopy (FTIR)   | 55 |

|          |   |    |
|----------|---|----|
| 2.11.6   | $^{13}\text{C}$ solid state nuclear magnetic resonance analysis ( $^{13}\text{C}$ -NMR) | 56 |
| 2.11.7   | UV-Visible diffuse reflectance spectroscopy (DRS)                                       | 56 |
| 2.11.8   | Photoluminescence spectroscopy (PLS) analysis   | 57 |
| 2.11.9   | pH-Potentiometric titration   | 57 |
| 2.11.10  | Swelling index (SI)   | 58 |
| 2.11.11  | Leaching ratio (LR) measurements  | 59 |
| 2.11.12  | Ionic conductivity measurement  | 59 |
| 2.12     | Evaluation of the photocatalytic performance  | 60 |
| 2.12.1   | Preparation of slurry $\text{TiO}_2$  | 60 |
| 2.12.2   | Testing the photocatalytic activity   | 61 |
| 2.12.3   | Testing the photocatalytic efficiency   | 62 |
| 2.12.4   | The Effect of pH  | 63 |
| 2.12.5   | Identification and determination of phenol's intermediates                              | 64 |
| 2.12.6   | Mineralization rate   | 64 |
| 2.12.6.1 | COD testing for organic binders   | 64 |
| 2.12.6.2 | COD testing for organic pollutants  | 65 |
|          | <b>CHAPTER THREE- RESULTS AND DISSCUSSION:</b>  | 66 |
|          | <b>Characterization and fabrication of <math>\text{TiO}_2</math>/CS based systems</b>   |    |
| 3.1      | Characterization of the chitosan and its cross-linked derivatives                       | 66 |
| 3.1.1    | Determination of the degree of deacetylation of CS flakes                               | 66 |
| 3.1.2    | FTIR spectral analysis of CS and its cross-linked derivatives                           | 68 |

|         |  |            |
|---------|--|------------|
| 3.1.3   | Elemental analysis (CHN)   | 71         |
| 3.1.4   | TEM micrographs  | 72         |
| 3.1.5   | Swelling index (SI) measurements   | 73         |
| 3.1.6   | Chemical oxygen demand (COD) test  | 74         |
| 3.1.7   | Photoluminescence spectroscopy (PLS) spectral analysis   | 75         |
| 3.1.8   | Ionic conductivity   | 77         |
| 3.2     | Fabrication and optimization of the bilayer TiO <sub>2</sub> /CS system                              | 79         |
| 3.2.1   | Loading of TiO <sub>2</sub> -ENR <sub>50</sub> formulation   | 79         |
| 3.2.2   | Loading of CS  | 81         |
| 3.2.3   | Effect of pH   | 85         |
| 3.2.4   | The effect of PF Loading in TiO <sub>2</sub> -ENR <sub>50</sub> formulation                          | 87         |
| 3.3     | Generation of macro pores on the TiO <sub>2</sub> layer  | 93         |
| 3.3.1   | SEM micrographs  | 96         |
| 3.3.2   | TGA and EDX analyses   | 96         |
| 3.3.3   | Chemical oxygen demand (COD) test  | 101        |
| 3.3.4   | The role of macro pores  | 106        |
| 3.3.4.1 | Enhancing the diffusion of water pollutants  | 106        |
| 3.3.4.2 | Enhancing the diffusion of hydroxyl radicals to the interface of TiO <sub>2</sub> /CS layers         | 108        |
|         | <b>CHAPTER FOUR- RESULTS AND DISSCUSSION:<br/>Photocatalytic-oxidation of CS and its derivatives</b> | <b>110</b> |
| 4.0     | Introduction   | 110        |

|        |   |     |
|--------|---|-----|
| 4.1    | Physicochemical characterizations of the photocatalytically-oxidized CS | 111 |
| 4.1.1  | Leaching ratio (LR) measurements  | 111 |
| 4.1.2  | Swelling index (SI) measurements  | 112 |
| 4.1.3  | pH-potentiometric titration   | 113 |
| 4.1.4  | Elemental analysis (CHN)  | 116 |
| 4.1.5  | FTIR spectral analysis  | 117 |
| 4.1.6  | <sup>13</sup> C NMR spectral analysis                                   | 118 |
| 4.1.7  | UV-Visible DRS spectral analysis  | 121 |
| 4.1.8  | Photoluminescence spectroscopy (PLS) spectral analysis                  | 122 |
| 4.1.9  | Surface morphology of CS  | 123 |
| 4.1.10 | Change in visual color  | 124 |
| 4.1.11 | Mechanistic discussion  | 126 |
| 4.2    | Physicochemical characterizations of photocatalytically-oxidized CS-ECH | 129 |
| 4.2.1  | Swelling index (SI) measurements  | 129 |
| 4.2.2  | pH-potentiometric titration   | 129 |
| 4.2.3  | Elemental analysis (CHN)  | 132 |
| 4.2.4  | FTIR spectral analysis  | 133 |
| 4.2.5  | <sup>13</sup> C NMR spectral analysis                                   | 136 |
| 4.2.6  | UV-Visible DRS spectral analysis  | 137 |
| 4.2.7  | Photoluminescence spectroscopy (PLS) spectral analysis                  | 139 |
| 4.2.8  | Change in visual color  | 140 |
| 4.2.9  | SEM micrographs   | 140 |
| 4.2.10 | Mechanistic discussion  | 142 |



|       |  |     |
|-------|--|-----|
| 4.3   | Physicochemical characterizations of photocatalytically-oxidized CS-GLA  | 144 |
| 4.3.1 | Swelling index (SI) measurements   | 144 |
| 4.3.2 | pH-potentiometric titration  | 144 |
| 4.3.3 | Elemental analysis (CHN)   | 147 |
| 4.3.4 | FTIR spectral analysis   | 148 |
| 4.3.5 | <sup>13</sup> C NMR spectral analysis  | 151 |
| 4.3.6 | UV-vis DRS spectral analysis   | 152 |
| 4.3.7 | Photoluminescence spectroscopy (PLS) spectral analysis   | 153 |
| 4.3.8 | Change in visual color   | 154 |
| 4.3.9 | Mechanistic discussion   | 156 |
|       | <b>CHAPTER FIVE- RESULTS AND DISSCUSSION:<br/>Photocatalytic performance of the bilayer systems for phenol removal</b> | 158 |
| 5.0   | Introduction   | 158 |
| 5.1   | Photoluminescence spectroscopy (PLS) spectral analysis   | 159 |
| 5.2   | Photocatalytic activity and reusability  | 162 |
| 5.3   | Control test and photocatalytic efficiency for phenol removal  | 166 |
| 5.4   | Identification of phenol's intermediates   | 168 |
| 5.5   | Photocatalytic efficiency for phenol's intermediate removal  | 171 |
| 5.6   | Mineralization of phenol and its intermediates   | 179 |
| 5.7   | Proposed mechanism of the photocatalytic degradation of phenol   | 181 |

|  |     |
|--|-----|
| <b>CHAPTER SIX: CONCLUSIONS AND<br/>RECOMMENDATIONS FOR FUTURE WORKS</b> | 183 |
| <b>6.1 Conclusions</b>   | 183 |
| <b>6.2 Recommendations for future works</b>                              | 189 |
| <b>REFERENCES</b>  | 190 |
| <b>APPENDICES</b>  | 209 |
| <b>LIST OF PUBLICATIONS AND CONFERENCES</b>                              | 216 |

## LIST OF TABLES

|  | Page |
|--|------|
| Table 1.1: Photocatalytic processes of immobilized TiO <sub>2</sub> under UV light.  | 16   |
| Table 1.2: Key properties of chitosan (Crini and Badot, 2008).   | 27   |
| Table 3.1: Assignment of the infrared bands of CS flakes.  | 69   |
| Table 3.2: Elemental content of CS and its cross-linked derivatives.   | 72   |
| Table 3.3: Swelling index (SI) of CS, CS-ECH and CS-GLA layers.  | 74   |
| Table 3.4: Measurements of bulk impedance and its corresponding ionic conductivity of un-irradiated CS, CS-ECH and CS-GLA single layers and irradiated CS, CS-ECH and CS-GLA sub-layers in the bilayer TiO <sub>2</sub> /CS, TiO <sub>2</sub> /CS-ECH and TiO <sub>2</sub> /CS-GLA system respectively, for 5 cycles of irradiation in 10 mg L <sup>-1</sup> phenol solutions. | 78   |
| Table 3.5: The pseudo first-order rate constants, their respective correlation coefficient and COD analysis of the photocatalytic-degradation of 20 mL 10 mg L <sup>-1</sup> phenol solution by bilayer TiO <sub>2</sub> /CS system as a function of CS layer loading. The deposited TiO <sub>2</sub> layer was fixed at 1.30 ± 0.08 mg cm <sup>-2</sup> .                     | 83   |
| Table 3.6: Percentage of carbon and weight loss in TiO <sub>2</sub> single layer and TiO <sub>2</sub> top layer in the bilayer TiO <sub>2</sub> /CS, TiO <sub>2</sub> /CS-ECH and TiO <sub>2</sub> /CS-GLA systems during the photocatalytic process by using TGA and EDX analyses.  | 103  |
| Table 4.1: Elemental content of un-irradiated CS single layer, irradiated CS single layer and irradiated CS sub-layer with TiO <sub>2</sub> in the bilayer TiO <sub>2</sub> /CS system for several repeated cycles of irradiation.   | 116  |
| Table 4.2: Elemental content of crosslinked CS-ECH as a single layer and/or a sub-layer in the bilayer TiO <sub>2</sub> /CS-ECH system under different cycles of irradiation.  | 133  |
| Table 4.3: Elemental content of cross-linked CS-ECH as a single layer and/or a sub-layer in the bilayer TiO <sub>2</sub> /CS-GLA system under different cycles of irradiation.   | 148  |

|            |  |     |
|------------|--|-----|
| Table 5.1: | Pseudo first-order rate constant and correlation coefficient $R^2$ values for the photocatalytic-oxidation degradation of 20 mL 10 mg L <sup>-1</sup> phenol solution by different applied systems at several repeated cycles of applications at 25 °C.                          | 165 |
| Table 5.2: | The main intermediates formed during the photocatalytic-oxidation process of phenol by all applied photocatalyst systems of TiO <sub>2</sub> slurry mode, TiO <sub>2</sub> single layer system, bilayer TiO <sub>2</sub> /CS system and bilayer TiO <sub>2</sub> /CS-GLA system. | 172 |

## LIST OF FIGURES

|   | Page |
|---|------|
| Figure 1.1: Illustration of the main processes occurring on a semiconductor particle following the electronic excitation. Electron-hole pair recombination can occur at the surface (reaction (a)) or in the bulk (reaction (b)) of the semiconductors. At the surface of the particle, photogenerated electrons can reduce an electron acceptor A (reaction (c)) and photogenerated holes can oxidize an electron donor D (reaction (d)). The combination of reaction (c) and (d) presents the semiconductor sensitization of the general redox reactions (Mills and Hunte, 1997). | 3    |
| Figure 1.2: Photoinduced processes on TiO <sub>2</sub> (Carp et al., 2004).   | 5    |
| Figure 1.3: Crystal structures of (a) anatase, (b) rutile (b), and (c) brookite (Bokhimia et al., 2001).  | 7    |
| Figure 1.4: Various wastewater treatment technologies in environmental engineering (Chen et al., 2000).   | 8    |
| Figure 1.5: Illustration of the photo-induced formation mechanism of electron-hole pair in a semiconductor TiO <sub>2</sub> particle with the presence of water pollutant (P) and dissolved oxygen (Chong et al., 2010).  | 10   |
| Figure 1.6: Basic steps occur on the photocatalytic surface in heterogeneous catalytic reaction (Fogler, 1999).   | 13   |
| Figure 1.7: Preparation of ENR by performic epoxidation (Yoksan, 2008).   | 18   |
| Figure 1.8: Chemical structure of Novolac phenol-formaldehyde resins (Wei et al., 2007).  | 20   |
| Figure 1.9: Chemical structures of (a) cellulose, (b) chitin and (c) chitosan, (Kumar, 2000).   | 26   |
| Figure 1.10: Possible structure of (a) cross-linked chitosan-epichlorohydrine (CS-ECH) and (b) cross-linked chitosan-glutaraldehyde (CS-GLA) (Ngah et al., 2002a).  | 31   |
| Figure 1.11: Possible structures of photooxidized chitosan forms (Sionkowaka et al., (2005); Ulaski and Sonntag, 2000).   | 34   |
| Figure 1.12: A possible mechanism of phenol destruction on illuminated TiO <sub>2</sub> (Sobczynski et al., 2004).  | 38   |

|             |  |    |
|-------------|--|----|
| Figure 2.1: | Schematic diagram for fabricating bilayer systems.   | 47 |
| Figure 2.2: | Schematic diagram of the experimental irradiation system set-up: (a) 45-W fluorescent lamp, (b) glass photo-reactor cell, (c) applied immobilized photocatalyst of a single or bilayer system, (d) ultra-pure water or phenol solution, (e) aquarium pump, (f) direct reading air flowmeter, (g) PVC tube, (h) pasteur pipette and (i) scissor jack. | 50 |
| Figure 2.3: | Schematic diagram of the experimental set-up for the adsorption of RR4 and/or phenol. (a) applied immobilized photocatalyst of either single or bilayer system, (b) glass cell, (c) aqueous solution of RR4 and/or phenol, (d) pasteur pipette, (e) PVC tube, (f) direct reading air flowmeter and (g) aquarium pump.                                | 51 |
| Figure 3.1: | FTIR spectrum and the calculation procedure to determine the degree of deacetylation for CS flakes.  | 67 |
| Figure 3.2: | FTIR spectra of (a) CS flakes, (b) CS semi-soluble, (c) CS soluble, (d) and (e) cross-linked CS with epichlorohydrine (CS-ECH) and glutaraldehyde (CS-GLA) respectively.   | 70 |
| Figure 3.3: | TEM micrographs of (a) soluble CS sample and (b) semi-soluble CS sample.   | 73 |
| Figure 3.4: | COD ( $\text{mg L}^{-1}$ ) values of irradiated water samples representing the leachability of CS, CS-ECH and CS-GLA single layers during repeated cycles of irradiation.  | 75 |
| Figure 3.5: | Photoluminescence spectra of (a) CS, (b) CS-ECH and (c) CS-GLA single layers, at excitation wavelength 325 nm.   | 76 |
| Figure 3.6: | A plot of apparent first-order rate constant of the photocatalytic degradation of 20 mL $10 \text{ mg L}^{-1}$ phenol solution by bilayer $\text{TiO}_2/\text{CS}$ system as a function of the catalyst loading ( $\text{mg cm}^{-2}$ ). The immobilized CS sub layer on all plates was fixed at $0.65 \pm 0.08 \text{ mg cm}^{-2}$ .                | 79 |
| Figure 3.7: | A typical SEM micrograph based on the cross-sectional view of the $\text{TiO}_2$ layer showing the thickness of $\text{TiO}_2$ layer of $40.94 \pm 1.16 \text{ }\mu\text{m}$ obtained by deposition of $1.30 \pm 0.08 \text{ mg cm}^{-2}$ onto a glass plate, at $150\times$ magnification power.  | 81 |

|                 |  |    |
|-----------------|--|----|
| Figure 3.8:     | A plot of pseudo first-order rate constants of the photocatalytic-degradation of 20 mL 10 mg L <sup>-1</sup> phenol solution by bilayer TiO <sub>2</sub> /CS system as a function of CS sub-layer loading. The deposited TiO <sub>2</sub> layer was fixed at $1.30 \pm 0.08$ mg cm <sup>-2</sup> .   | 84 |
| Figure 3.9:     | A typical SEM micrograph based on the cross-sectional view of the CS layer showing the thickness of CS layer $6.35 \pm 0.61$ μm obtained by casting $0.65 \pm 0.08$ mg cm <sup>-2</sup> of CS solution onto glass plate.   | 85 |
| Figure 3.10:    | A plot of pseudo first-order rate constant of the photocatalytic-degradation of 20 mL 10 mg L <sup>-1</sup> phenol solution by bilayer TiO <sub>2</sub> /CS system as a function of various pH of phenol solution.   | 87 |
| Figure 3.11(a): | The effect of loading PF as a function of the percentage of the TiO <sub>2</sub> layer remained upon sonication time.  | 88 |
| Figure 3.11(b): | The effect of loading PF on the relative strength of the immobilized TiO <sub>2</sub> layer after 30 second of sonication time.  | 89 |
| Figure 3.12(a): | The effect of the CS sub-layer on the mechanical strength of the TiO <sub>2</sub> top layer with and without 0.15 g PF upon sonication time.   | 90 |
| Figure 3.12(b): | The effect of the CS sub-layer on the relative strength of the TiO <sub>2</sub> top layer with and without 0.15 g PF after 30 second of sonication time.   | 91 |
| Figure 3.13:    | A plot of pseudo first-order rate constant of the photocatalytic degradation of 20 mL 10 mg L <sup>-1</sup> phenol solution by bilayer TiO <sub>2</sub> /CS system as a function of PF loading (g), both immobilized CS and TiO <sub>2</sub> layers on all plates was fixed at $0.65 \pm 0.08$ mg cm <sup>-2</sup> and $1.30 \pm 0.08$ mg cm <sup>-2</sup> respectively. | 92 |
| Figure 3.14:    | A typical SEM micrograph based on the cross-sectional view of the CS-ECH layer showing the thickness of this layer at $4.81 \pm 0.07$ μm obtained by casting $0.65 \pm 0.08$ mg cm <sup>-2</sup> of CS-ECH solution onto a glass plate.  | 95 |
| Figure 3.15:    | A typical SEM micrograph based on the cross-sectional view of the CS-GLA layer showing the thickness of this layer at $5.23 \pm 0.04$ μm obtained by casting $0.65 \pm 0.08$ mg cm <sup>-2</sup> of CS-GLA solution onto a glass plate.  | 95 |

|              |  |     |
|--------------|--|-----|
| Figure 3.16: | Typical SEM micrographs of (a) un-irradiated TiO <sub>2</sub> single layer (b) after 3 cycles, (c) after 5 cycles and (d) after 10 cycles of irradiation in 20 mL ultra-pure water, at 5000× magnification power.  | 97  |
| Figure 3.17: | Typical SEM micrographs of (a) un-irradiated TiO <sub>2</sub> top layer in the TiO <sub>2</sub> /CS bilayer system, (b) after 3 cycles, (c) after 5 cycles and (d) after 10 cycles of irradiation in 20 mL ultra-pure water, at 5000× magnification power.   | 98  |
| Figure 3.18: | Typical SEM micrographs of (a) un-irradiated TiO <sub>2</sub> top layer in the TiO <sub>2</sub> /CS-ECH bilayer system, (b) after 3 cycles, (c) after 5 cycles and (d) after 10 cycles of irradiation in 20 mL ultra-pure water, at 5000× magnification power.   | 99  |
| Figure 3.19: | Typical SEM micrographs of (a) un-irradiated TiO <sub>2</sub> top layer in the TiO <sub>2</sub> /CS-GLA bilayer system, (b) after 3 cycles, (c) after 5 cycles and (d) after 10 cycles of irradiation in 20 mL ultra-pure water, at 5000× magnification power.   | 100 |
| Figure 3.20: | TGA and DTG curves of (a) ENR <sub>50</sub> , (b) PF, (c) and (d) TiO <sub>2</sub> top layer in the TiO <sub>2</sub> /CS bilayer system: [(i) before irradiation, (ii) after 3 cycles, (iii) after 5 cycles and (iv) after 10 cycles of irradiation in 20 mL ultra-pure water].  | 102 |
| Figure 3.21: | COD values of the irradiated water samples a function of the number of repeated cycles.  | 105 |
| Figure 3.22: | The percentage of anionic RR4 dye removed by adsorption on bilayer TiO <sub>2</sub> /CS systems.   | 107 |
| Figure 3.23: | UV-Vis DRS spectra of the RR4 dye saturated plates on (a) CS/glass (control plate), (b) CS sub-layer of the bilayer TiO <sub>2</sub> /CS system without pre-generated macro-pores after one cycle of irradiation, (c) and (d) CS sub-layers of the belayed TiO <sub>2</sub> /CS systems with pre-generated macro-pores after one cycle and five cycles of irradiation respectively. (e) CS sub-layer in the bilayer TiO <sub>2</sub> /CS system after five cycles of irradiation during the photocatalytic degradation of phenol without adsorbed RR4 dye. | 109 |
| Figure 4.1:  | Measuring the weight loss as a function of the leaching ratio (LR) of the irradiated CS single layer, irradiated bilayer TiO <sub>2</sub> /CS system, irradiated TiO <sub>2</sub> single layer and un-irradiated bilayer TiO <sub>2</sub> /CS system at different times of irradiation in ultra-pure water.  | 112 |



|                  |   |     |
|------------------|---|-----|
| Figure 4.2 (a):  | Typical pH-potentiometric titration curves of the un-irradiated CS single layer and irradiated CS sub-layer in the bilayer TiO <sub>2</sub> /CS system for 5 cycles of irradiation.   | 114 |
| Figure 4.2 (b):  | First order derivative plot based on pH-potentiometric titration curves of the un-irradiated CS single layer.   | 115 |
| Figure 4.2 (c):  | First order derivative plot based on pH-potentiometric titration curves of the irradiated CS sub-layer in the bilayer TiO <sub>2</sub> /CS system for 5 cycles.   | 115 |
| Figure 4.3:      | FTIR spectra of (a) un-irradiated CS single layer (b) irradiated CS single layer for 5 cycles of irradiation (c) irradiated CS sub-layer in the bilayer TiO <sub>2</sub> /CS system for 5 cycles in the presence of nitrogen gas, (d) irradiated CS sub-layer in the bilayer TiO <sub>2</sub> /CS system for 5 cycles in the presence of air and (e) irradiated CS sub-layer in the bilayer TiO <sub>2</sub> /CS system for 10 cycles in the presence of air. | 119 |
| Figure 4.4:      | <sup>13</sup> C NMR spectra of (a) un-irradiated CS single layer and (b) irradiated CS sub-layer in the bilayer TiO <sub>2</sub> /CS system for 5 cycles.   | 120 |
| Figure 4.5:      | UV-vis DRS spectra of (a) unirradiated CS single layer and (b) irradiated CS sub-layer in the bilayer TiO <sub>2</sub> /CS system for for 5 cycles.   | 121 |
| Figure 4.6:      | Photoluminescence spectra of (a) un-irradiated CS single layer and (b) irradiated CS sub-layer in the bilayer TiO <sub>2</sub> /CS system for 5 cycles, at excitation wavelength 325 nm.  | 123 |
| Figure 4.7:      | SEM micrographs of CS sub-layer in the bilayer TiO <sub>2</sub> /CS system (a) before and (b) after 5 cycles of irradiation, at 5000× magnification power.  | 124 |
| Figure 4.8:      | The photographs of (a) un-irradiated CS single layer and (b) irradiated CS sub- layer in the bilayer TiO <sub>2</sub> /CS system after 5 cycles of irradiation, after the complete removal of the TiO <sub>2</sub> top layer.   | 125 |
| Figure 4.9:      | The proposed structure of the photocatalytically-oxidized CS sub-layer in the bilayer TiO <sub>2</sub> /CS system.  | 128 |
| Figure 4.10 (a): | pH-potentiometric titration curves of un-irradiated CS-ECH single layer and irradiated CS-ECH sub-layer in the bilayer TiO <sub>2</sub> /CS-ECH system for 5 cycles.  | 130 |

|                   |  |     |
|-------------------|--|-----|
| Figure 4.10 (b):  | First order derivative plot based on pH-potentiometric titration curve of un-irradiated CS-ECH single layer.   | 131 |
| Figure 4.10 (c):  | First order derivative plot based on pH-potentiometric titration curves of irradiated CS-ECH sub-layer in the bilayer TiO <sub>2</sub> /CS system for 5 cycles.  | 131 |
| Figure 4.11:      | FTIR spectra of (a) un-irradiated CS-ECH single layer, (b) irradiated CS-ECH single layer for 5 cycles, (c) irradiated CS-ECH sub-layer in the bilayer TiO <sub>2</sub> /CS-ECH system for 5 cycles in the presence of nitrogen, (d) and (e) irradiated CS-ECH sub-layer in the bilayer TiO <sub>2</sub> /CS-ECH system in the presence of air for 5 and 10 cycles respectively. | 135 |
| Figure 4.12:      | <sup>13</sup> C NMR spectra of (a) un-irradiated CS-ECH single layer and (b) irradiated CS-ECH sub-layer in the bilayer TiO <sub>2</sub> /CS-ECH system for 5 cycles.  | 137 |
| Figure 4.13:      | UV-vis DRS spectra of (a) un-irradiated CS-ECH single layer and (b) irradiated CS-ECH sub-layer in the bilayer TiO <sub>2</sub> /CS-ECH system for 5 cycles.   | 138 |
| Figure 4.14:      | Photoluminescence spectra of (a) un-irradiated CS-ECH single layer and (b) irradiated CS-ECH sub-layer in the bilayer TiO <sub>2</sub> /CS-ECH system for 5 cycles.  | 139 |
| Figure 4.15:      | The photographs of (a) a photo can be presented un-irradiated CS-ECH single layer, irradiated CS-ECH single layer for 5 cycles and irradiated CS-ECH sub-layer in the bilayer TiO <sub>2</sub> /CS-ECH system for 5 cycles in the presence of nitrogen, and (b) irradiated CS-ECH sub-layer in the bilayer TiO <sub>2</sub> /CS-ECH system for 5 cycles in the presence of air.  | 141 |
| Figure 4.16:      | SEM micrographs of CS-ECH sub-layer in the bilayer TiO <sub>2</sub> /CS-ECH system (a) before and (b) after five cycles of irradiation, at 5000× magnification power.  | 142 |
| Figure 4.17:      | Proposed structure of the photocatalytically-oxidized CS-ECH sub-layer in the bilayer TiO <sub>2</sub> /CS-ECH system.   | 143 |
| Figure 4. 18 (a): | pH-potentiometric titration curves of un-irradiated CS-GLA single layer and irradiated CS-GLA sub-layer in the bilayer TiO <sub>2</sub> /CS-GLA system for 5 cycles.   | 145 |
| Figure 4. 18 (b): | First order derivative plot based on pH-potentiometric titration curve of un- irradiated CS-GLA single layer.  | 146 |

|                  |  |     |
|------------------|--|-----|
| Figure 4. 18(c): | First order derivative plot based on pH-potentiometric titration curves of irradiated CS-GLA sub-layer in the bilayer TiO <sub>2</sub> /CS-GLA system for 5 cycles.  | 146 |
| Figure 4.19:     | FTIR spectra of (a) un-irradiated CS-GLA single layer, (b) irradiated CS-GLA single layer for 5 cycles, (c) irradiated CS-GLA sub-layer in the bilayer TiO <sub>2</sub> /CS-GLA system for 5 cycles in the presence of nitrogen, (d) and (e) irradiated CS-GLA sub-layer in the bilayer TiO <sub>2</sub> /CS-GLA system in the presence of air for 5 and 10 cycles respectively. | 150 |
| Figure 4.20:     | <sup>13</sup> C NMR spectra of (a) un-irradiated CS-GLA single layer and (b) irradiated CS-GLA sub-layer in the bilayer TiO <sub>2</sub> /CS-GLA system for 5 cycles in the presence of air.   | 152 |
| Figure 4.21:     | UV-vis DRS spectra of (a) un-irradiated CS-GLA single layer, (b) irradiated CS-GLA sub-layer in the bilayer TiO <sub>2</sub> /CS-GLA system for 5 cycles.  | 153 |
| Figure 4.22:     | Photoluminescence spectra of (a) un-irradiated CS-GLA single layer and (b) irradiated CS-GLA sub-layer in the bilayer TiO <sub>2</sub> /CS-GLA system for 5 cycles.  | 154 |
| Figure 4.23:     | The photographs of (a) un-irradiated CS-GLA single layer and (b) irradiated CS-GLA sub-layer in the bilayer TiO <sub>2</sub> /CS-GLA system for 5 cycles respectively.   | 155 |
| Figure 4.24:     | The proposed structure of the photocatalytically-oxidized CS-GLA sub-layer in the bilayer TiO <sub>2</sub> /CS-GLA system.   | 157 |
| Figure 5.1:      | Photoluminescence spectra of un-irradiated (a) TiO <sub>2</sub> single layer system, (b) bilayer TiO <sub>2</sub> /CS system, (c) bilayer TiO <sub>2</sub> /CS-ECH system and (d) bilayer TiO <sub>2</sub> /CS-GLA system.   | 159 |
| Figure 5.2:      | Photoluminescence spectra of irradiated (a) TiO <sub>2</sub> single layer system, (b) bilayer TiO <sub>2</sub> /CS system, (c) bilayer TiO <sub>2</sub> /CS-GLA system and (d) bilayer TiO <sub>2</sub> /CS-ECH system, for 5 cycles of irradiation in 10 mg L <sup>-1</sup> phenol solution.  | 160 |
| Figure 5.3:      | A plot of pseudo first-order rate constant as a function to the photocatalytic activity for removal of 20 mL 10 mg L <sup>-1</sup> phenol by different applied systems at several repeated cycles of irradiation.  | 162 |

|                 |  |     |
|-----------------|--|-----|
| Figure 5.4:     | Percentage of 10 mg L <sup>-1</sup> phenol remained as a function of contact time by using various treatment methods of adsorption, direct photolysis and photocatalytic-oxidation processes.                                  | 166 |
| Figure 5.5:     | HPLC chromatogram and retention time (min) of degraded phenol with its main intermediate products generated after 30 minutes of the photocatalytic-oxidation process in the presence of the TiO <sub>2</sub> in a slurry mode. | 169 |
| Figure 5.6:     | HPLC chromatogram and retention time of the individual pure standards of MAL, FUM, HQ, CAT and PhOH.   | 170 |
| Figure 5.7:     | HPLC chromatogram and retention time of the mixture of pure standards of MAL, FUM, HQ, CAT and PhOH before spiking into the degraded phenol solution of Figure 5.5.  | 170 |
| Figure 5.8:     | HPLC chromatogram and retention time (min) of the mixture of pure standards of MAL, FUM, HQ, CAT and PhOH of Figure 5.7, after spiking into the degraded phenol solution of Figure 5.5.  | 172 |
| Figure 5.9 (a): | Intermediates formed and its representative HPLC chromatogram during the photocatalytic-oxidation of phenol by using TiO <sub>2</sub> in slurry mode.  | 173 |
| Figure 5.9 (b): | Intermediates formed and its representative HPLC chromatogram during the photocatalytic-oxidation of phenol by using TiO <sub>2</sub> single layer system.   | 174 |
| Figure 5.9 (c): | Intermediates formed and its representative HPLC chromatogram during the photocatalytic-oxidation of phenol by bilayer TiO <sub>2</sub> /CS system.  | 175 |
| Figure 5.9 (d): | Intermediates formed and its representative HPLC chromatogram during the photocatalytic-oxidation of phenol by bilayer TiO <sub>2</sub> /CS-GLA system.  | 176 |
| Figure 5.9 (e): | Intermediates formed and its representative HPLC chromatogram during the photocatalytic-oxidation of phenol by bilayer TiO <sub>2</sub> /CS-ECH system.  | 177 |
| Figure 5.10:    | COD analysis versus irradiation time was taken as a function of mineralization rates of 20 mg L <sup>-1</sup> phenol solution by different systems.  | 180 |

Figure 5.11:      The possible reaction mechanism of the photocatalytic-oxidation of phenol.      182

## LIST OF ABBREVIATIONS AND SYMBOLS

|                      |   |
|----------------------|---|
| a. u.                | Arbitrary units                                 |
| AOPs                 | Advance oxidation processes                     |
| $^{13}\text{C}$ -NMR | $^{13}\text{C}$ Nuclear Magnetic Resonance      |
| CHN                  | Carbon, Hydrogen and Nitrogen elemental content |
| COD                  | Chemical Oxygen Demand                          |
| CS                   | Chitosan  |
| CS-ECH               | Cross-linked chitosan- epichlorohydrin          |
| CS-GLA               | Cross-linked chitosan- glutaraldehyde           |
| $e^-$                | Negative electron                               |
| e-beam               | Electron- beam                                  |
| $E_{bg}$             | Energy band gap                                 |
| ECH                  | Epichlorohydrin                                 |
| EDX                  | Energy Dispersive X-ray                         |
| FTIR                 | Fourier-transform infrared spectroscopy         |
| GLA                  | Glutaraldehyde                                  |
| $h^+$                | Positive hole                                   |
| $h\nu$               | Photonic energy                                 |
| $k_{app}$            | Apparent (pseudo) first-order rate constant     |
| L-H                  | Langmuir-Hinshelwood                            |
| LR                   | Leaching ratio                                  |
| LUMO                 | lowest unoccupied molecular orbital             |
| NHE                  | Normal hydrogen electrode                       |
| PF                   | Phenol Formaldehyde resin                       |
| PLS                  | Photoluminescence spectrum                      |
| SEM                  | Scanning Electron Microscopy                    |
| SI                   | Swelling Index                                  |
| TEM                  | Transmission Electron Microscopy                |
| TGA                  | Thermal gravimetric analysis                    |
| UV                   | Ultraviolet                                     |
| UV-Vis DRS           | UV-Visible diffuse reflectance spectroscopy     |
| VB                   | Valence band                                    |
| V-UV                 | Vacuum-ultraviolet                              |
| $\Omega$             | Ohm   |

**PENGOKSIDAAN PEMFOTOMANGKIN KITOSAN DAN TERBITANNYA  
DAN FENOL OLEH TiO<sub>2</sub> TERIMOBILASASI MELALUI SISTEM  
SUSUNAN DUA LAPISAN DIBAWAH SINARAN CAHAYA NAMPAK**

**ABSTRAK**

Sistem dwilapisan mudah yang terdiri daripada TiO<sub>2</sub> sebagai lapisan atas dan kitosan (CS), rangkai silang kitosan-gluteraldehid (CS-GLA) dan kitosan-epiklorohidrin (CS-ECH) sebagai lapisan bawah telah berjaya dihasilkan dan dipegunkan pada plat kaca. Sifat-sifat pemendapan dan kelekatan TiO<sub>2</sub> dapat diperbaiki dengan menambah pengikat organik seperti getah asli terepoksi (ENR<sub>50</sub>) dan resin fenol-formaldehid (PF) di dalam formulasi penyaduran. Apabila sistem dwilapisan ini melalui proses sinaran di dalam larutan akueus yang diudarakan di bawah 45-W lampu pendarfluor telah menyebabkan perubahan yang ketara terhadap kandungan kedua-dua ENR<sub>50</sub> dan PF pada lapisan atas TiO<sub>2</sub>, selain daripada perubahan fizik-kimia yang istimewa pada lapisan bawah CS, CS-GLA dan CS-ECH. Walau bagaimanapun, telah didapati bahawa semasa fotodegradasi sebahagian daripada ENR<sub>50</sub> dan PF telah bertindak sebagai agen pembentukan liang untuk menghasilkan bukaan liang pada permukaan TiO<sub>2</sub> seperti yang tunjukkan oleh analisis SEM, sementara analisis TGA, EDX dan ujian COD pula menunjukkan secara kuantitatifnya tiada perubahan yang signifikan terhadap kandungan ENR<sub>50</sub> dan PF yang boleh didapati selepas 5 kitaran penggunaan berulang. Struktur berongga lapisan TiO<sub>2</sub> terpegun ini membenarkan penyebaran pencemar dengan lebih efektif, meningkatkan penembusan cahaya dan memperbaiki sifat optik seperti yang ditunjukkan oleh analisis spektroskopi fotopendarcahaya (PLS).

Sementara itu, lapisan bawah CS, CS-GLA dan CS-ECH teroksidasi secara perlahan dalam 5 kitaran penggunaan berulang. Kajian pencirian melalui analisis unsur, spektroskopi inframerah transformasi fourier (FT-IR), spektroskopi resonans magnet nukleus keadaan pepejal  $^{13}\text{C}$ , spektroskopi pemantulan bauran UV-Sinar nampak (DRS), spektroskopi fotopendarcahaya (PLS) dan ukuran pengembangan secara lazimnya menunjukkan pembentukan kumpulan karbonil dan penyingkiran sebahagian daripada kumpulan amino tanpa mengubah sebahagian besar struktur polimer CS dan terbitan rangkaisilangnya. Dalam semua kes, warna lapisan CS telah dilihat bertukar menjadi lebih keperangan dan pengambilan air telah berkurangan. Pembentukan serentak pembukaan liang pada permukaan  $\text{TiO}_2$  dan pengoksidaan lapisan bawah CS, CS-GLA dan CS-ECH bertanggungjawab terhadap pengurangan kadar penggabungan semula pasangan lubang elektron di permukaan lapisan atas  $\text{TiO}_2$ . Akibatnya, berdasarkan pada pemalar kadar tertib pertama seperti yang diperolehi daripada analisis HPLC, aktiviti pemangkinan foto oleh sistem yang digunakan untuk penyingkiran fenol mematuhi urutan seperti berikut  $\text{TiO}_2/\text{CS-ECH} > \text{TiO}_2/\text{CS-GLA} > \text{TiO}_2/\text{CS} \geq \text{rampaian TiO}_2 > \text{TiO}_2 \text{ lapisan tunggal}$ . Perubahan yang sama telah diperolehi untuk kecekapan pemangkinan foto dan kadar mineralisasi bagi fenol dan bahan perantaraannya seperti asid maleik, asid fumarik, hidrokuinon dan katekol. Kesan penjerapan boleh diabaikan dan kesemua sistem terpegun ini boleh diguna semula untuk sekurang-kurangnya 10 kitaran tanpa kehilangan keaktifannya.



# **PHOTOCATALYTIC OXIDATION OF CHITOSAN AND ITS DERIVATIVES AND PHENOL BY IMMOBILIZED TiO<sub>2</sub> BILAYER ASSEMBLAGE SYSTEMS UNDER VISIBLE LIGHT**

## **ABSTRACT**

Simple bilayer systems consisting of TiO<sub>2</sub> as a top layer and chitosan (CS), cross-linked chitosan-glutaraldehyde (CS-GLA) and chitosan-epichlorohydrin (CS-ECH) as sub-layers were successfully fabricated and immobilized onto a glass plate. The deposition and adhesive properties of TiO<sub>2</sub> were improved by adding organic binders like epoxidized natural rubber (ENR<sub>50</sub>) and phenol-formaldehyde resin (PF) in the coating formulation. Exposing these bilayer systems in aerated aqueous solution to 45-W fluorescent lamp caused significant changes in content of both ENR<sub>50</sub> and PF of TiO<sub>2</sub> top layer, in addition to the remarkable physico-chemical changes of CS, CS-GLA and CS-ECH sub-layers. However, it was found that the ENR<sub>50</sub> and PF had actually acted as pore-forming agents via their photodegradation process to create macro pores on the TiO<sub>2</sub> surface as shown by SEM analysis, while TGA, EDX and COD analyses indicated quantitatively that there is no significant change in ENR<sub>50</sub> and PF content that can be observed after 5 cycles of repeated usage. This porous structure of immobilized TiO<sub>2</sub> layer allows better diffusion of pollutants, increases the light penetration and improves the optical property as indicated by photoluminescence spectroscopy (PLS) analysis.

CS, CS-GLA and CS-ECH sub-layers were mildly oxidized within 5 cycles (Each cycle was equivalent to two hours of irradiation) of repeated usage. Characterization studies via elemental analysis, Fourier-transform infrared spectroscopy (FTIR), <sup>13</sup>C solid state nuclear magnetic resonance (<sup>13</sup>C-NMR), UV-

Visible diffuse reflectance spectroscopy (DRS), photoluminescence spectroscopy (PLS) analyses and swelling measurement generally indicated the formation of carbonyl group and partial elimination of some amino groups without altering much of the whole polymeric structure of CS and its cross-linked derivatives. In all cases, the visual color of sub-layers of CS and its cross-linked derivatives had converted to more intense brown and less water uptake was also observed. The simultaneous generation of macro pores on TiO<sub>2</sub> surface and oxidation of CS, CS-GLA and CS-ECH sub-layers are responsible for the reduction in the recombination rate of electron-hole pair on the surface of TiO<sub>2</sub> top layer. Consequently, according to the pseudo first-order rate constant as determined by HPLC analysis shows that the photocatalytic activity of applied systems for phenol removal followed this order TiO<sub>2</sub>/CS-ECH > TiO<sub>2</sub>/CS-GLA > TiO<sub>2</sub>/CS ≥ TiO<sub>2</sub> in slurry > TiO<sub>2</sub> single layer. The same trend was observed for photocatalytic efficiency and mineralization rate for phenol and its intermediates, which were identified to be maleic acid, fumaric acid, hydroquinone and catechol. In fact, the effect of adsorption was extremely negligible and all these immobilized systems were reusable at least for up to 10 cycles of applications without losing their photocatalytic activity.

## CHAPTER ONE

### INTRODUCTION

#### 1.1 Photocatalysis

The phenomenon of photocatalysis can be defined as the combination of photochemistry and catalysis. More precisely, the meaning of “photocatalysis” herein implies direct interaction between the light and catalyst (Hamal and Klabunde, 2007). Therefore, there is no photoreaction on illumination with light alone. Thus, reaction usually demands the use of photocatalyst which implies that the photon assists the generation of catalytically active species (Chatterjee and Dasgupta, 2005).

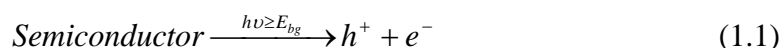
However, all the knowledge that was acquired during the development of semiconductor photoelectrochemistry during 1970 and 1980s had significantly enhanced the development of photocatalysis (Heller, 1981). The application of photocatalysis, especially photocatalysis using semiconductor particles, is an emerging new scientific technology. This is especially true after the discovery by Fujishima and Honda of the photolysis of water into environmentally clean fuels (hydrogen and oxygen) utilizing an electrode of titanium dioxide ( $\text{TiO}_2$ ) in an electrochemical cell (Fujishima and Honda, 1972). Following this, several works have been devoted solely towards understanding the essential concept of the photocatalysis process for enhancing the photocatalytic efficiency as well as investigating the overall advantages of the photocatalytic process for the environmental remediation technologies. Hence, several advantages can be concluded from applying this technology in environmental protection, which are listed as follows (Kabra et al., 2004):

- a. Photocatalysis exhibits an alternative way for the energy-intensive traditional treatment methods with great capability of harvesting renewable and pollution-free solar energy.
- b. Photocatalysis technology does not require transformation of treated pollutants from one medium to another, unlike conventional treatments methods.
- c. High capability for destroying a wide range of hazardous compounds in different wastewater streams.
- d. Potentially applicable to aqueous and gaseous-phase treatment, as well as to some extent solid (soil) phase treatments.
- e. The photo-reaction conditions for photocatalysis in general are mild, the photodegradation time is modest, and less chemical agents input are required.
- f. The generated intermediates of treated hazardous compounds are minimal.
- g. The photocatalyst (semiconductor) powder is recoverable and reusable for many cycles of treatment.

## **1.2 Fundamental mechanism of photocatalysis**

Unlike metals which already have a continuum of electronic state, semiconductors possess a void energy region without energy levels that are available to promote the recombination of an electron and hole generated by photoactivation in the solid semiconductors. The void region that centered between the top of the filled valence band (VB) and the bottom of the vacant conduction band (CB) is called energy band gap ( $E_{bg}$ ) (Linsebigler et al., 1995). The process of semiconductors photocatalysis basically includes the following steps. If the energy of the incident photon is equal or exceeds the band gap energy ( $E_{bg}$ ) of the semiconductors/

photocatalyst, absorption of the photonic energy ( $h\nu$ ) by the semiconducting solids leads to excitation of an electron ( $e^-$ ) from the valence band to the conduction band of the semiconductor and a positive hole ( $h^+$ ) would be left in the valence band. Ultraviolet (UV) or near-UV photons are typically needed for this type of photoreaction (Mills and Hunte, 1997).



Thus, the generated pair ( $e^-$ - $h^+$ ) immediately migrates to the semiconductor/photocatalyst surface where they either recombine, producing wasted-thermal energy or take place in subsequent reduction and oxidation (redox) processes with any compound, which might be adsorbed on the photocatalyst surface to give the necessary end-products (Chatterjee and Dasgupta, 2005; Kabra et al., 2004). The overall mechanism of the photo-induced semiconductor/photocatalyst is illustrated in Figure 1.1 (Mills and Hunte, 1997).

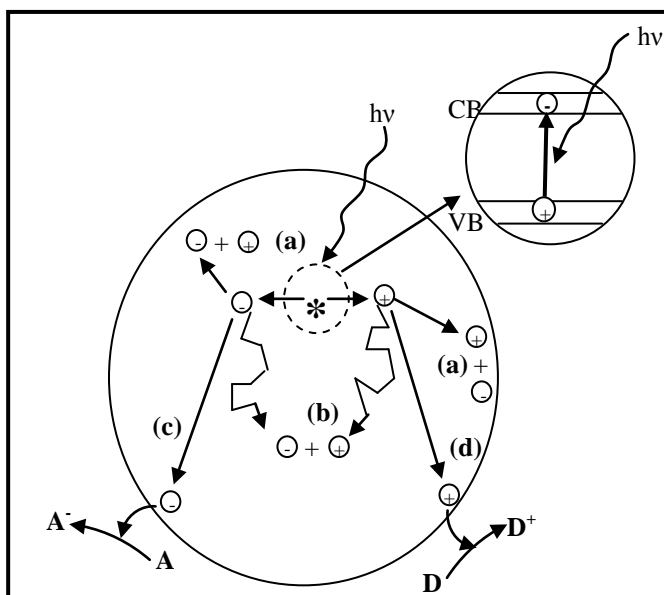


Figure 1.1: Illustration of the main processes occurring on a semiconductor particle following the electronic excitation. Electron-hole pair recombination can occur at the surface (reaction (a)) or in the bulk (reaction (b)) of the semiconductors. At the surface of the particle, photogenerated electrons can reduce an electron acceptor A (reaction (c)) and photogenerated holes can oxidize an electron donor D (reaction (d)). The combination of reaction (c) and (d) presents the semiconductor sensitization of the general redox reactions (Mills and Hunte, 1997).

Several types of semiconductor catalyst such as  $\text{TiO}_2$ ,  $\text{ZnO}$ ,  $\text{ZnS}$ ,  $\text{CdS}$ ,  $\text{Fe}_2\text{O}_3$  and  $\text{GaP}$  have been tested as photocatalysts for the degradation of a wide range of ambiguous refractory organic pollutants into harmless biodegradable compounds, and finally mineralize them to  $\text{CO}_2$ ,  $\text{H}_2\text{O}$  and other mineral acids. Among all of the semiconductors catalysts, titanium dioxide,  $\text{TiO}_2$ , is close to being an ideal benchmark photocatalyst in the environmental photocatalysis applications (Chong et al., 2010).

The various applications of  $\text{TiO}_2$  in the photocatalysis technology include selective synthesis of organic compound (Pillai and Endalkachew, 2002), photokilling of pathogenic organism (Sichel et al., 2007), cancer treatment (Fujishima et al., 2000), self-cleaning and anti-fogging (Fujishima and Zhang, 2006), air cleaning (Sun et al., 2003), detoxification and remediation of water (Dominguez et al., 2005), degradation of hazardous inorganic compounds (Kim et al., 1998), decontamination of soil (Hamerski et al., 1999) and treatment of heavy metals (Eliet and Bidoglio, 1998). In addition to the unique characteristic of  $\text{TiO}_2$  in the wide range of applications mentioned above, it also offers unlimited applications by the presence of photoinduced phenomenon which is depicted in Figure 1.2 (Carp et al., 2004).

### **1.3 $\text{TiO}_2$ as semiconductor photocatalyst**

#### **1.3.1 General remarks of $\text{TiO}_2$**

Titanium dioxide ( $\text{TiO}_2$ ) is one of the members of transition metal oxides. In the beginning of the 20th century, titanium dioxide was used intensively in industrial products in order to replace the older toxic lead oxides as pigments for white paint. Recently, the yearly production of  $\text{TiO}_2$  passed 4 million tons. This pigment has been

widely used in various applications involving paint, plastics, rubber, inks, papers and textile, in addition to the considerable amount of the global production used in food and pharmaceuticals products (Carp et al., 2004).

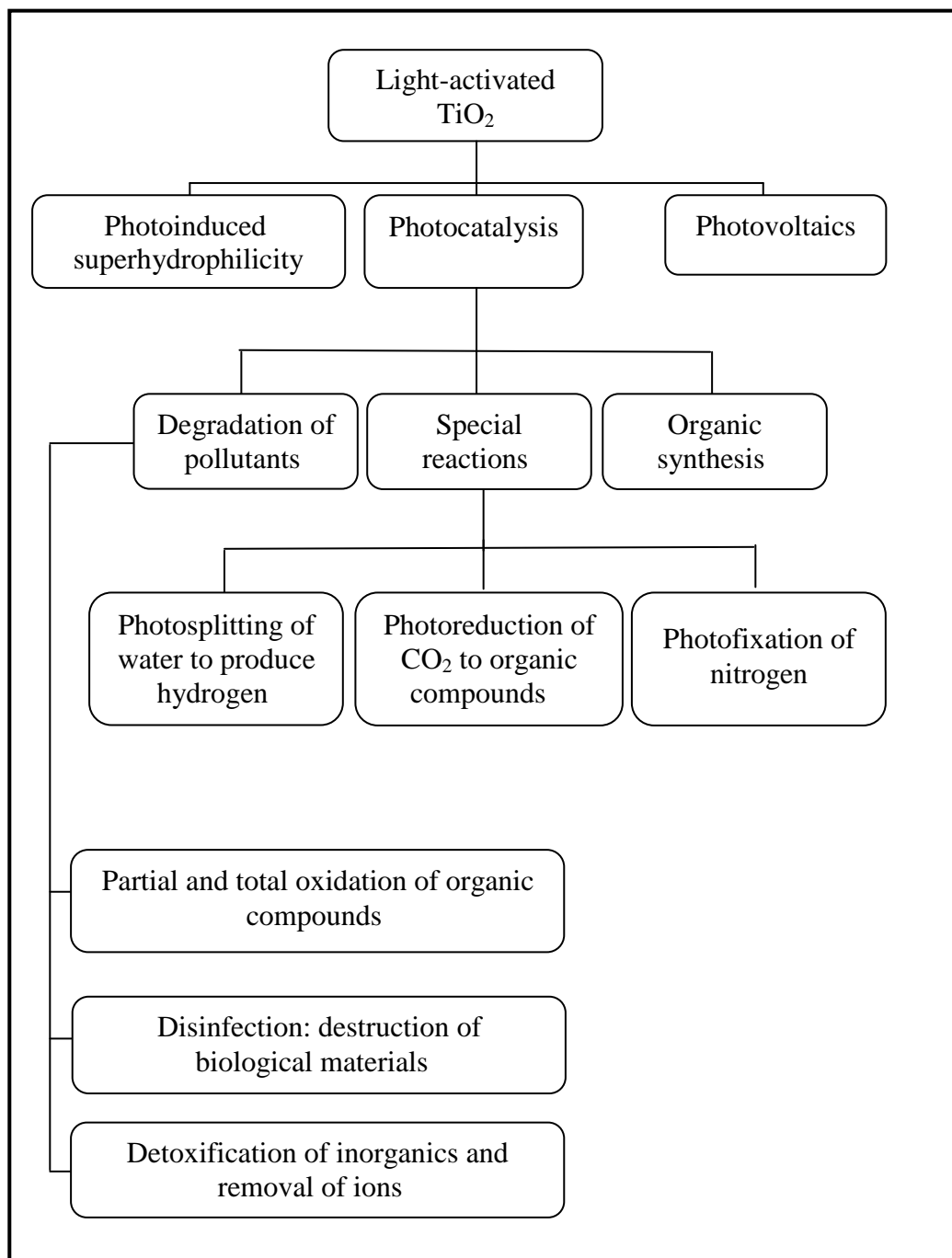


Figure 1.2: Photoinduced processes on  $\text{TiO}_2$  (Carp et al., 2004).

In fact, there are two possible ways to manufacture the commercial  $\text{TiO}_2$  pigments, either by sulfate or chloride processes. The sulfate process involves direct reaction between the  $\text{TiO}_2$  ore and sulfuric acid; then the product is hydrolyzed to produce a hydrate oxide, which is followed by calcination process at  $900\text{ }^\circ\text{C}$  to obtain pigmentary  $\text{TiO}_2$  (Delgado-Vargas and Paredes-Lopez, 2003). The chloride process was improved in 1920 but not commercially applicable until the late 1950s. In this process,  $\text{TiO}_2$  ore reacts with gaseous chlorine in the presence of coke to produce liquid titanium tetrachloride. The product is distilled and oxidized in the vapor phase to obtain pigmentary  $\text{TiO}_2$  (Blakey and Hall, 1988).

### **1.3.2 Crystallographic structure of $\text{TiO}_2$**

In nature,  $\text{TiO}_2$  crystallizes in three crystalline forms: anatase (its name is derived from the Greek word ‘anatsis’ meaning ‘extension’), rutile (its name is derived from the Latin word ‘rutilus’ meaning ‘red’) and brookite (its name is named in honor of the English mineralogist, H.J. Brooke). These crystal structures are classified based on the  $\text{TiO}_2^{6-}$  octahedral unit (Carp et al., 2004).

However, anatase type  $\text{TiO}_2$  has a crystalline structure that matches the tetragonal system (with dipyramidal habit) and is employed basically as a photocatalyst in UV light region. The rutile type  $\text{TiO}_2$  has a tetrahedral symmetry structure (with prismatic habit) which is mainly utilized as whitening pigment of paint. As for brookite type  $\text{TiO}_2$ , it has an orthorhombic crystalline structure. All the crystalline forms of  $\text{TiO}_2$  are depicted in Figure 1.3 (Bokhimia et al., 2001).



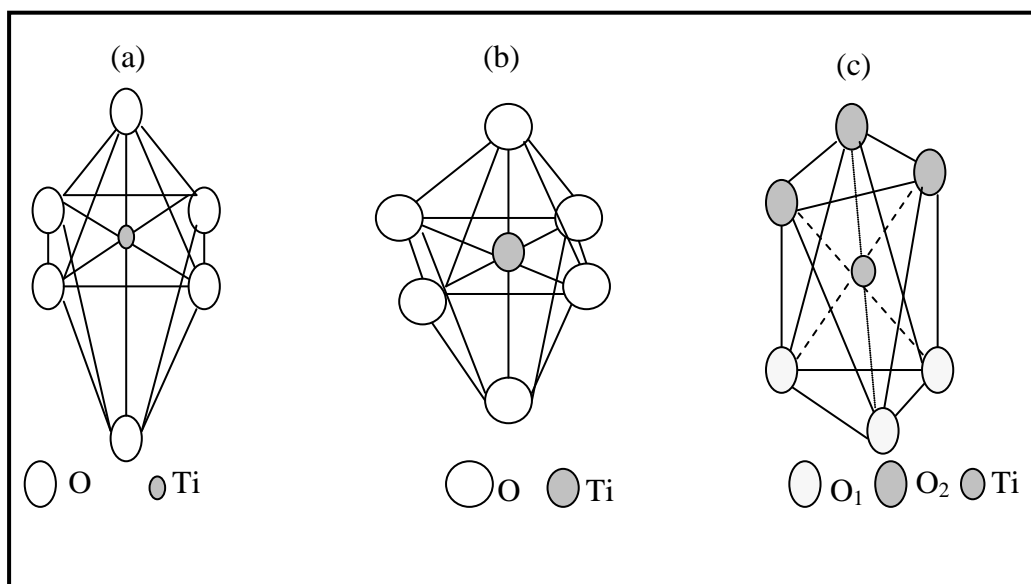


Figure 1.3: Crystal structures of (a) anatase, (b) rutile (b), and (c) brookite (Bokhimia et al., 2001).

#### 1.4 Heterogeneous TiO<sub>2</sub> photocatalysis

Among many different types of advanced oxidation processes (AOPs) are UV, VUV, O<sub>3</sub>/UV, O<sub>3</sub>/V-UV, H<sub>2</sub>O<sub>2</sub>/UV, Fenton (Fe<sup>2+</sup>/H<sub>2</sub>O<sub>2</sub>), Fenton-like (Fe<sup>3+</sup>/H<sub>2</sub>O<sub>2</sub>), photo-Fenton reactions and heterogeneous photocatalysis TiO<sub>2</sub>/UV, TiO<sub>2</sub>/UV/H<sub>2</sub>O<sub>2</sub> and TiO<sub>2</sub>/UV/O<sub>3</sub> (Dominguez et al., 2005). Heterogeneous photocatalyst using TiO<sub>2</sub> as one of the advance oxidation processes (AOPs) has received great attention from the environmental standpoint in comparison with other AOPs as well as the conventional wastewater technologies. The conventional and AOPs technologies are summarized in Figure 1.4 (Chen et al., 2000). However, the heterogeneous photocatalyst is potentially applicable for destruction of a wide spectrum of organic and inorganic water contaminants at ambient pressure and temperature in a relatively short time period without production of polycyclic products. It is also capable of oxidizing pollutants in ppb ranges and only requires oxygen as an oxidizing agent (Carp et al., 2004).

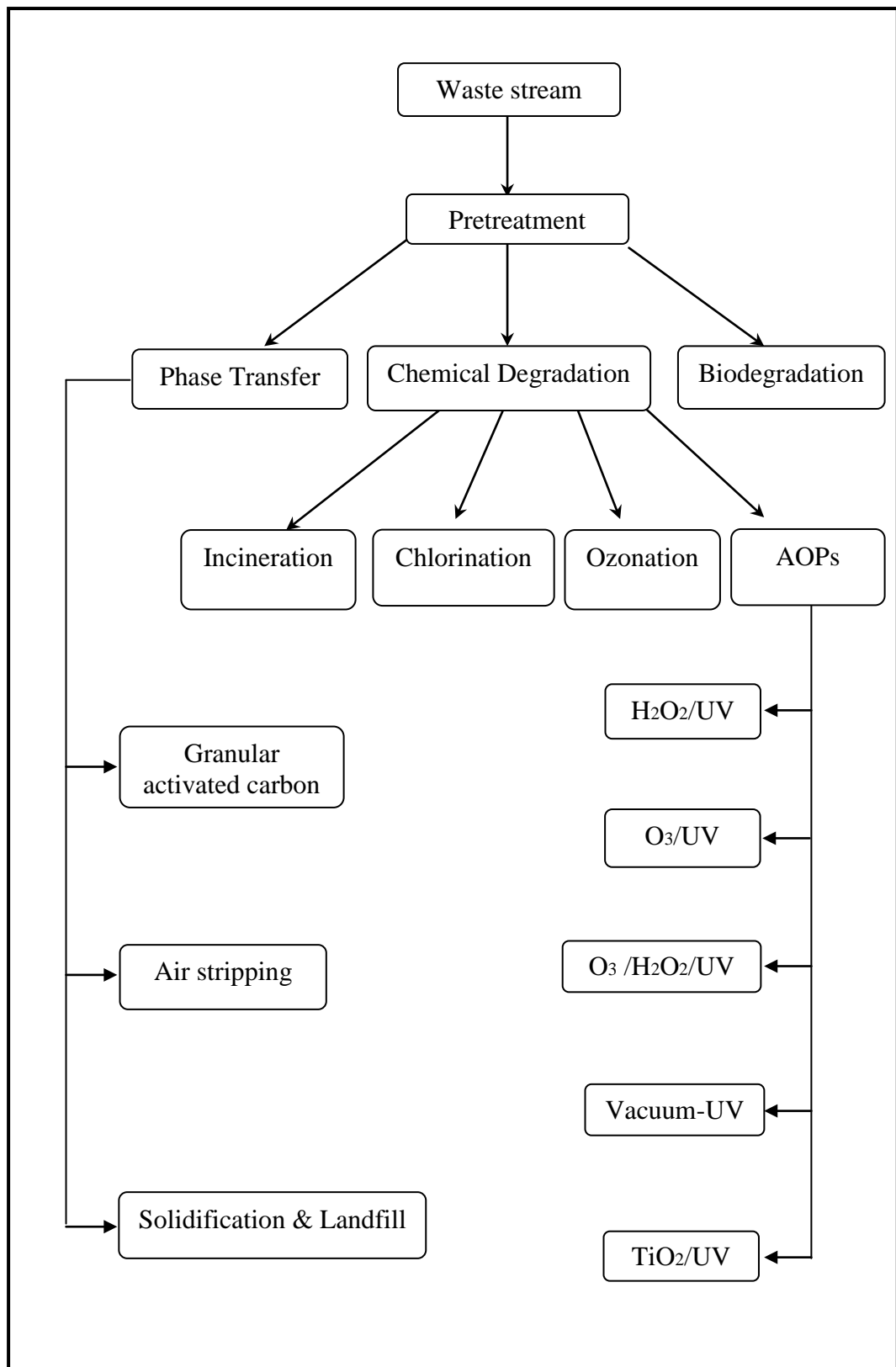


Figure 1.4: Various wastewater treatment technologies in environmental engineering (Chen et al., 2000).

As generally observed,  $\text{TiO}_2$  is close to being an ideal photocatalyst and well-researched material in the environmental photocatalysis applications because of its many desirable properties such as follows (Mills and Hunte, 1997):

- a.** Inexpensive and readily available.
- b.** Biologically and chemically inert.
- c.** Having broad spectral absorption response in the UV-C (220-290 nm), UV-B (290-320 nm) and UV-A (320-400 nm) with high absorption coefficient.
- d.** Photoactive.
- e.** Photostable (i.e. not liable to photoanodic corrosion for instance).

The process of photocatalytic reaction by  $\text{TiO}_2$  takes place by the absorption of ultraviolet (UV) or near-ultraviolet photons ( $h\nu$ ) that is equal or exceed the band gap energy ( $E_{bg}$ ) value for anatase 3.2 eV, or 3.0 eV for rutile onto its surface. An electron would be photoexcited from the valence band (VB) to the empty conduction band (CB) of the  $\text{TiO}_2$  and a positive hole would be left in the valence band in femtoseconds. Subsequently, a series of reductive and oxidative reactions will be induced on the  $\text{TiO}_2$  surface. The overall mechanism of the electron-hole pair formation as well as the redox reactions involving various compounds adsorbed on the photocatalyst surface when  $\text{TiO}_2$  is irradiated with adequate  $h\nu$  is depicted in Figure 1.5 (Chong et al., 2010). The series of chain oxidative-reductive reactions (Equations (1.2) – (1.12)) that take place at the photoinduced  $\text{TiO}_2$  surface was generally proposed as follows (Chong et al., 2010):

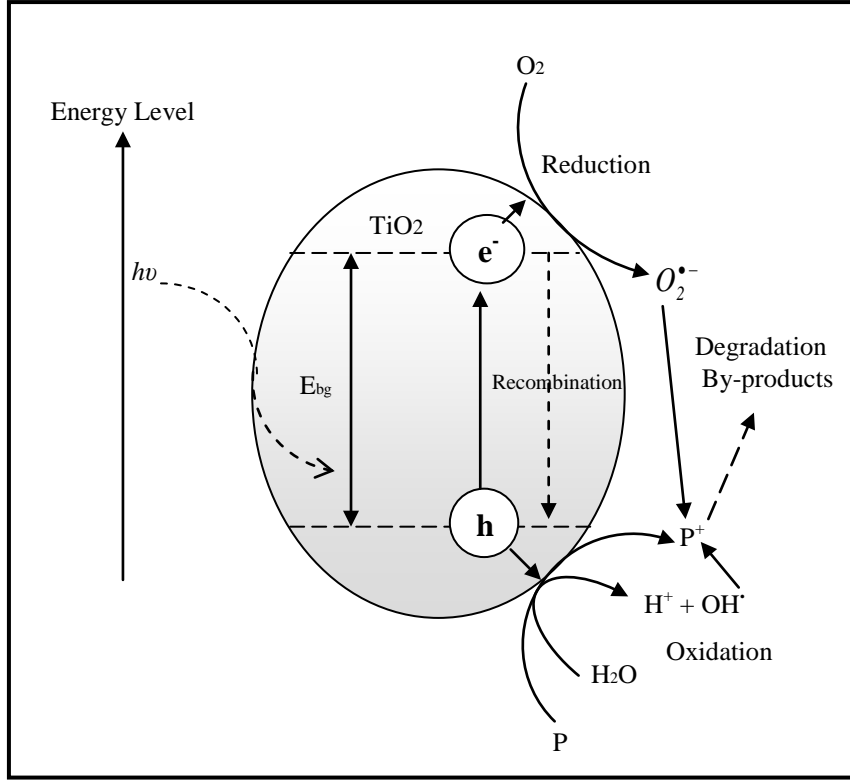
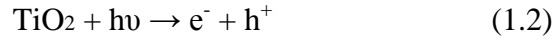


Figure 1.5: Illustration of the photo-induced formation mechanism of electron-hole pair in a semiconductor  $\text{TiO}_2$  particle with the presence of water pollutant (P) and dissolved oxygen (Chong et al., 2010).

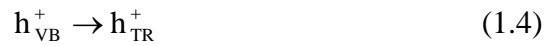
Photoexcitation :



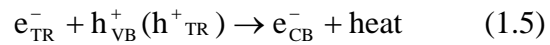
Charge-carrier trapping of  $e^-$  :



Charge-carrier trapping of  $h^+$  :



Electron-hole recombination:



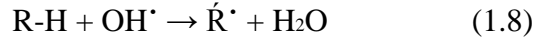
Photoexcited e<sup>-</sup> scavenging:



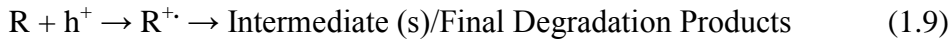
Oxidation of hydroxyls:



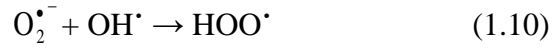
Photodegradation by  $\text{OH}^\bullet$  :



Direct photoholes:



Protonation of superoxides:



Co-scavenging of  $\text{e}^-$  :



Formation of  $\text{H}_2\text{O}_2$  :



The  $\text{e}_{\text{TR}}^-$  and  $\text{h}_{\text{TR}}^+$  in Equation 1.4 represent the surface trapped valence band electron and conduction band hole respectively. In this regard, it was found that these trapped carriers are usually bound to the  $\text{TiO}_2$  surface and do not recombine immediately after photo excitation (Furube et al., 2001). The absence of the electron scavengers leads to direct recombination between the photoexcited electron and the valence band hole in nanosecond with simultaneous release of heat energy (Equation 1.5). On the other hand, the presence of electron scavengers like oxygen is important for prolonging the recombination rate and successful functioning of

photocatalytic performance. Equation 1.6 shows how necessary the presence of oxygen is in preventing the direct recombination of electron-hole pair, while allowing the formation of superoxides radical ( $O_2^{\bullet-}$ ). This  $O_2^{\bullet-}$  radical would be further protonated to produce the hydroperoxyl radical ( $HO_2^{\bullet}$ ) and subsequently producing hydrogen peroxide ( $H_2O_2$ ) as presented in Equations 1.10 and 1.11 respectively.

However, all these occurrences in photocatalysis reactions are dependant totally on the presence of both dissolved oxygen and water molecules. In fact, without the presence of water molecules, the highly reactive hydroxyl radicals ( $OH^{\bullet}$ ) could not be generated and impede the photocatalytic reaction of liquid phase organic pollutants (Chong et al., 2010). In other words, the fundamental task of the heterogenous photocatalyst is to generate free radicals in the solution, mainly the highly reactive hydroxyl radical ( $OH^{\bullet}$ ), which is traditionally responsible for oxidizing almost all organic pollutants to  $CO_2$ ,  $H_2O$  and simple mineral acids because of its high standard reduction potential of 2.8 V vs. NHE, being exceeded only by fluorine (Carp et al., 2004). Thus, during the heterogeneous photocatalytic reactions, the dissolved organic pollutants are degraded to its corresponding intermediates and subsequently mineralized to carbon dioxide and water, if the photo-treatment time is extended (Equation 1.13) (Chong et al., 2010).



The overall photocatalysis reaction as depicted by Equation 1.13 can be divided into five individual steps, which are depicted in Figure 1.6 and detailed out as follows (Fogler, 1999):

- a. Movement of the organic pollutant(s) (e.g. A) from the aqueous solution to the  $\text{TiO}_2$  surface.
- b. Adsorption process of the organic pollutant(s) onto the photoinduced  $\text{TiO}_2$  surface (i.e. surface activation by absorption photonic energy occurs simultaneously in this step).
- c. Photocatalysis reaction for the adsorbed phase of organic pollutant(s) on the  $\text{TiO}_2$  surface (e.g.  $A \rightarrow B$ ).
- d. Desorption of the intermediate(s) (e.g. B) from the  $\text{TiO}_2$  surface.
- e. Movement of the intermediate(s) (e.g. B) from the interface region to the bulk fluid.

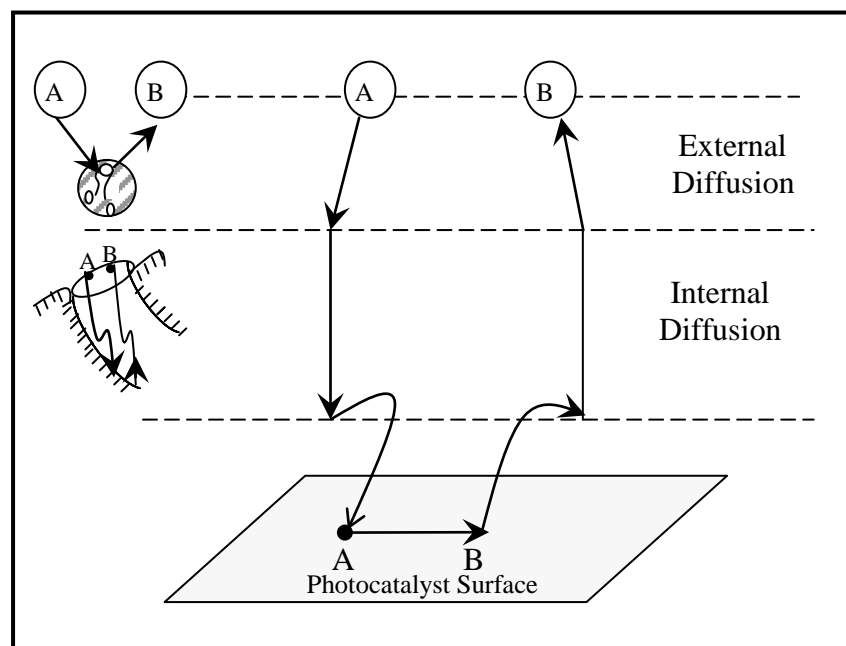


Figure 1.6: Basic steps that occur on the photocatalytic surface in heterogeneous catalytic reaction (Fogler, 1999).

However, it must be noted that the anatase form is the most active allotropic form. For instance, rutile is thermodynamically more stable than anatase, but anatase formation is kinetically preferable at temperature conditions lower than 600 °C.

Consequently, this lower temperature could offer higher surface area and higher surface density of active sites for pollutants adsorption and for catalytic process (Herrmann, 1999). In fact, rutile type  $\text{TiO}_2$  possess a relatively lower band gap energy value of 3.0 eV as opposed to 3.2 eV for anatase and the spectral absorption response of light can also extend to the visible light region, but anatase  $\text{TiO}_2$  shows better photocatalytic performance with maximum quantum yield better than the rutile  $\text{TiO}_2$  due to its conduction band position which demonstrates stronger reduction power as compared to the rutile  $\text{TiO}_2$  (Puma et al., 2008).

In spite of the various advantages obtained from photocatalysis based on  $\text{TiO}_2$ , heterogeneous photocatalysis for water treatment is still in the developmental stages as some significant challenges remain to be solved before effective applications can even be contemplated. Thus, in order to develop this technology into a cost-effective treatment and as a viable alternative to the current technologies, more fundamental research is needed in order to broaden the spectral response of  $\text{TiO}_2$  to visible or solar spectrum and also to solve the post-treatment catalyst powder recovery (Chong et al., 2010).

## **1.5 Immobilization of $\text{TiO}_2$ photocatalyst**

In heterogeneous photocatalyst technology, there are two major designs of heterogeneous photoreactor systems, one in which the  $\text{TiO}_2$  powder is used in the suspension or slurry mode and another in which it is immobilized on an appropriate solid support or on the inner wall of a photoreactor. The majority of the early photoreactors have used  $\text{TiO}_2$  powder suspended in contaminated water, since it presents high surface area for the photocatalytic reaction to take place and provides almost no mass transfer limitation (Damodar and Swaminathan, 2008).



In fact, the slurry systems normally pose several practical problems of post-treatment catalyst recovering step. This final step is normally a very difficult, costly, energy and time consuming process. The  $\text{TiO}_2$  suspended particles have great tendency to aggregate especially at high concentrations. The particles may also cause the scattering of incident UV light resulting in serious difficulty in applying it to the continuous flow system (Andronic and Duta, 2008; Zhang et al., 2007).

Thus, immobilization of  $\text{TiO}_2$  powder on solid supports is an alternative and convenient method to solve these problems. Even though the photocatalytic efficiency of the immobilized  $\text{TiO}_2$  system may be less than that of the slurry system due to the reduced surface area accessible for photocatalytic reaction as well as low porosity of the supported catalyst layer (Mascolo et al., 2007), but the catalyst can be used for long-term applications without lowering much of its photocatalytic efficiency (Dionysiou et al., 2000; Fabiyi and Skelton, 2000). The summary of some of the supporting materials as well as some deposition methods that are reported in the literatures are shown in Table 1.1.

In order to avoid the cracking and fast peeling off of catalyst layer after short period of usage (Gelover et al., 2004), various deliberate steps should be taken into account in a careful selection of the catalyst deposition parameters that may yield high quality immobilized catalyst in terms of high adhesion properties, and high photocatalytic performance due to high porosity of the immobilized catalyst surface (Andronic and Duta, 2008). The catalyst support should be chemically inert in order to avoid any additional source of water pollution coming from the leaching of the metals ions into the treated solution, in case of using metal substrates as the supporting materials. The same environmental problems would be faced when inorganic adhesives are used as binders for the photocatalyst powder.

Table 1.1 Photocatalytic processes of immobilized TiO<sub>2</sub> under UV light

| References               | Pollutant degraded                    | Deposition method                               | Support material                         |
|--------------------------|---------------------------------------|---|--|
| Uddin et al., 2007       | Methylene blue                        | Sol-gel   | Cellulose fiber                          |
| Tryba, 2008              | Phenol                                | Manual pasted with a brush                      | Cotton material                          |
| Andronic and Duta, 2008  | Methyl orange                         | Doctor blade                                    | Microscopy glass substrate               |
| Zhang et al., 2007       | Phenol                                | Vapor hydrolysis method                         | Tetrapod-like ZnO                        |
| Tasbihi et al., 2007     | Phenol                                | Sol-gel   | Glass beads, silica gel, and quartz sand |
| Nikolaki et al., 2006    | 1,3-dichloro-2-propanol               | Spray technique using pipetting                 | Reactor tubular wall                     |
| Horikoshi et al., 2002   | Nonylphenol polyethoxylate surfactant | Dip-coating                                     | Fiberglass cloth                         |
| Chen and Dionysiou, 2006 | 4-chlorobenzoic acid                  | Modified sol-gel                                | Stainless steel                          |
| Li et al., 2008          | Methyl orange                         | Dropping TiO <sub>2</sub> solution onto zeolite | Zeolite                                  |
| Hosseini et al., 2007    | Phenol                                | Direct mixing                                   | Perlite                                  |
| Kansal et al., 2008      | Lignin                                | Spray gun                                       | Pumice stone                             |
| Chen et al., 2006        | Benzene                               | Plasma sprayed                                  | Aluminum                                 |
| Fabiyi and Skelton, 2000 | Methylene blue                        | Thermal treatment                               | Polystyrene beads                        |
| Watts and Cooper, 2008   | 4-chlorophenol                        | Direct mixing                                   | Concrete surfaces                        |

Table 1.1: Continued

|                               |                                    |                                 |                               |
|-------------------------------|------------------------------------|---------------------------------|-------------------------------|
| Damodar and Swaminathan, 2008 | Azo dye                            | Smooth paint brush              | PVC tube                      |
| Yao et al., 2010              | Phenol and methyl orange           | Sol-gel-adsorption              | Activated carbon              |
| Mascolo et al., 2007          | Methyl red                         | Rotary evaporating              | Cylindrical glass             |
| Kim et al., 2005              | <i>S. choleraesuis</i> subsp       | Drop into catalyst formulation  | Chitosan beads                |
| Wang et al., 2002             | Trichloroethane                    | Chemical vapor deposition (CVD) | Pyrex glass tube              |
| Dionysiou et al., 2000        | Chlorinated phenols and pesticides | Sol-gel                         | Stainless steel rotating disk |
| Fretwell and Doglas, 2001     | 4-Chlorophenol                     | Dip or spin-coating             | Quartz or glass               |
| Brezova et al., 1997          | Phenol                             | Sol-gel                         | Glass fibers                  |

## 1.6 Organic binders

### 1.6.1 Epoxidized natural rubber (ENR)

Natural rubber (NR) has been commonly used as an economic adhesive material for various products such as tires, products under the car bonnet, gloves, balloons, rubber bands, etc, due to its unique physico-chemical characteristics such as elasticity, stickiness and resilience. However, the great limitations of NR is due to its chemical structure (cis 1,4-polyisoprene) as shown in Figure 1.7, which exhibits low stability to heat, sunlight and oxygen (Yoksan, 2008). The chemical modification of NR is one of the promising ways to modify a part of the carbon-carbon double bonds on the molecular structure of NR into the polar epoxy group and eventually producing epoxidized natural rubber (ENR). The epoxidation process

leads to the reduction of the molecular weight of NR with an increase in the density of the ENR produced. The resultant ENR offers excellent air impermeability, oil and organic solvent proof, wet road grip performance and wide spread applications (Yoksan, 2008; Yu et al., 2008). In general, the preparation of ENR is usually performed by the epoxidation of NR with peracetic, perbenzoic and perphtallic acids in solution (Hong and Chan, 2004). However, the epoxidation process utilizes an in-situ technique based on hydrogen peroxide and formic acid in order to epoxidize NR latex. The preparation steps are depicted in Figure 1.7 (Yoksan, 2008). The Malaysian Rubber Board presently provides two types of ENR, which are namely ENR<sub>25</sub> and ENR<sub>50</sub>. The number in each of their name indicates the degree of epoxidation with 25 and 50 mol % of epoxide group's in the ENR molecules. Thus, the properties of glass transition temperature ( $T_g$ ), oil resistance and melt viscosity increased when the epoxide content of ENR increased as well (Thongnuanchan et al., 2007).

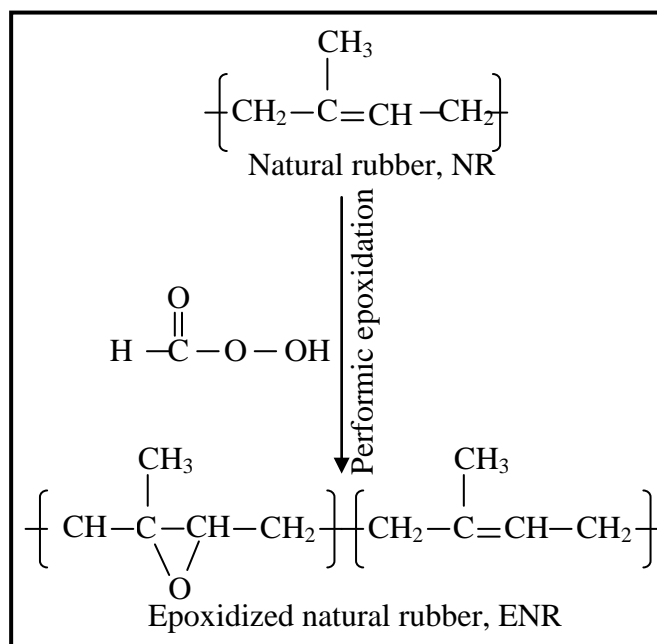


Figure 1.7: Preparation of ENR by performic epoxidation (Yoksan, 2008).

In heterogeneous photocatalyst technology, ENR<sub>50</sub> had been successfully used as a good emulsifier with PVC in order to improve the distribution of catalyst in the coating formulation and therefore, enhancing the coating properties of TiO<sub>2</sub> photocatalyst on the solid substrate for the photocatalytic degradation of methylene blue (Shin, 2010). Furthermore, ENR<sub>50</sub> had also acted as adhesives to strengthen the coating conditions of the immobilized TiO<sub>2</sub> in the presence of phenol-formaldehyde resin on various solid supports for photocatalytic degradation of methylene blue and cibacron brilliant red dyes (Amar, 2006). Finally, addition of ENR<sub>50</sub> into immobilizing solution had improved the adhesiveness and robustness of the coated TiO<sub>2</sub> as well as significantly speeded up the immobilization process of TiO<sub>2</sub> on the aluminum plate by electrophoretic deposition technique for the photocatalytic degradation of phenol (Nawi et al., 2003).

### **1.6.2 Phenol-formaldehyde (PF) resin**

Phenol-formaldehyde (PF) resin is one of the oldest synthetic polymers synthesized in 1907 from the chemical reaction of phenol with formaldehyde. It is also considered the first true thermosetting synthetic polymer and presents many desirable properties such as the resistance of heat, corrosion, wear and the excellent mechanics adhesive capacity (Wanga et al., 2009). However, there are mainly two types of phenol-formaldehyde resins that had been synthesized with different formaldehyde/phenol ratios, namely Novolac and Resol. The phenolic resin composition depends on monomer ratio, catalyst, reaction conditions, and residual free monomers. Furthermore, the temperature and pH conditions play a significant role in the reaction of phenols with formaldehyde and eventually determine the profile and characteristics of the Novolac or Resol resin. Thus, phenol-formaldehyde

resin of novolac type is produced in acidic pH whereas Resol type is produced in alkaline conditions with an excess molar ratio of formaldehyde ( $1 < \text{formaldehyde/phenol} < 3$ ) (Poljansek and Krajnc, 2005). The Novolac resin is a linear chain condensation product, which normally produces a nonporous dense layer. The typical chemical structure of novolac phenol-formaldehyde resin is depicted in Figure 1.8 (Wei et al., 2007). In recent years, huge amounts of PF has been consumed in the wood industry in USA, Japan, China and some European countries due to its high bonding strength, excellent water resistance and chemical stability (Jin et al., 2010). Moreover, a combination of PF and ENR<sub>50</sub> proved to be an excellent coating formulation of TiO<sub>2</sub> powder in heterogeneous photocatalyst technology (Amar, 2006).

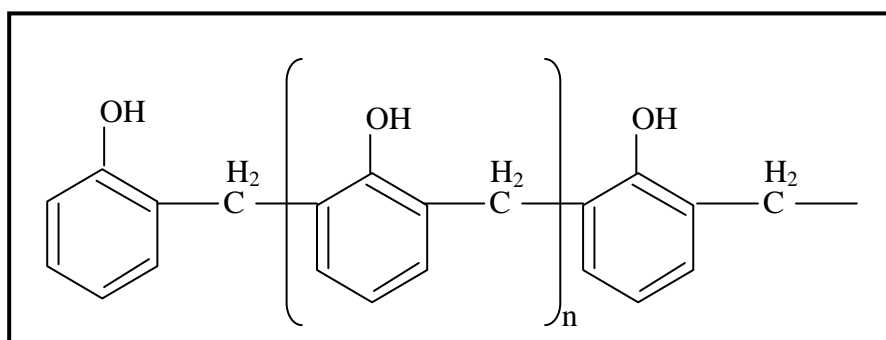


Figure 1.8: Chemical structure of Novolac phenol-formaldehyde resins (Wei et al., 2007).

### 1.7 Modification of TiO<sub>2</sub> by conventional methods

Several attempts have been made in order to solve one of the major challenges related to the relatively wide band gap of TiO<sub>2</sub> which absorbs only 3-4 % energy of the solar spectrum and restricts its applications due to the need of an UV excitation source (Hamal and Klabunde, 2007). Therefore, further development of

TiO<sub>2</sub> should consider meeting the requirements of large-scale applications of TiO<sub>2</sub> by harvesting more solar energy or increasing its spectral sensitivity towards visible light region. Enhancing the photocatalytic performance of the TiO<sub>2</sub> has been achieved by several conventional approaches as discussed below.

### **1.7.1 Self-sensitization by using colored pollutants**

Organic dyestuffs with visible light absorbing chromophores are responsible for photosensitizing TiO<sub>2</sub> photocatalyst in the field of treating textile wastewater. By this means, the irradiation of adsorbed dye on the TiO<sub>2</sub> surface by visible light leads to the ejection of an electron from the photo-excited dye to the conduction band of TiO<sub>2</sub> photocatalyst. Consequently, the presence of electron scavengers like oxygen leads to the formation of superoxide radical anion, which attacks the dye repeatedly to mineralize it to non-toxic harmless end product(s) (Bauer et al., 2001). The disadvantages of this method come from its limitation for the dyestuff or textile dyes only. The photocatalytic activity that depends basically on the adsorption rate of dyes which is an irreversible process that could cause blocking of the active sites on the catalyst surface and higher photocatalytic performance that demands for the nano-scale TiO<sub>2</sub> particles (Nagaveni et al., 2004).

### **1.7.2 Dyes modifying TiO<sub>2</sub>**

Dye sensitization approach depends basically on the anchoring of pigments on the surface of TiO<sub>2</sub> photocatalyst which follows the same concept of self-sensitization mentioned in Section 1.7.1. The high photocatalytic performance of the modified TiO<sub>2</sub> photocatalyst is attributed to the photoinjection of an electron from the conduction band of the excited pigment anchored on the photocatalyst particles to

the conduction band of the TiO<sub>2</sub> support. Consequently, the quantum yield of the redox process would be increased due to the additional formation of superoxides radical O<sub>2</sub><sup>•-</sup> generated on the TiO<sub>2</sub> conduction band (Iliev, 2002). However, the photocatalytic efficiency of the dyes doping system to the TiO<sub>2</sub> photocatalyst depends on many factors such as the conduction band edge of the semiconductor, the LUMO (lowest unoccupied molecular orbital) of the dye, population of the low lying ligand fields, and the presence of the adsorbates such as water vapor and oxygen (Ozcan et al., 2007).

### **1.7.3 Doping of TiO<sub>2</sub> with metal ions**

Doping of TiO<sub>2</sub> lattice with a series of metal ions such as V, Cr, Mn, Fe, Ni, etc., causes a red shift in the absorption pattern of TiO<sub>2</sub> photocatalyst. This phenomenon is basically due to the creation of local energy levels of metal ions within the band gap of the TiO<sub>2</sub> photocatalyst. Thus, the electronic properties of the TiO<sub>2</sub> become modified to a large extent and the photocatalyst shows clear response in the visible light region (Anpo and Takeuchi, 2003; Serpone et al., 1994). In fact, the preparation method plays an important role in the photocatalytic efficiency of prepared photocatalyst. Therefore, inserting different types of metal ions into TiO<sub>2</sub> lattice leads to different photocatalytic efficiencies. In some cases there is no photocatalytic activity noticed under visible light and lower activity even in the UV light region compared to non-doped photocatalysts. This retardation in the photocatalytic activity comes from high rate of recombination of charge carriers through the metal ion energy levels (Brezova et al., 1997; Fujishima and Zhang, 2006). Furthermore, doping of metal ions involves other drawbacks related to the thermal instability of the doped TiO<sub>2</sub>, high-cost of ion-implantation facilities, and



fast electron trapping by the metal centers (Wang et al., 1999; Yamashita et al., 1998).

#### **1.7.4 Doping of TiO<sub>2</sub> with non-metal atoms**

Doping of TiO<sub>2</sub> lattice with non-metal atoms such as N (Kosowska et al., 2005), F (Mrowetz and Selli, 2006), S (Periyat et al., 2008), and C (Xiao et al., 2008) is considered as another widespread technological approach for enhancing the photocatalytic activity of TiO<sub>2</sub> by narrowing its band gap for larger absorption in the visible light region. For instance, narrowing band gap of N-doped TiO<sub>2</sub> can be achieved by substituting oxygen with nitrogen in the TiO<sub>2</sub> lattice. As a result, the corresponding N (2p) states are centered above the valence band edge. Hence, mixing of N (2p) states with O (2p) states leads to the reduction of the band gap of the N-doped TiO<sub>2</sub> and higher photocatalytic activity for the degradation of color and colorless pollutants can be achieved under visible light irradiation (Kosowska et al., 2005). Additionally, the photocatalytic activity of carbon-doped TiO<sub>2</sub> can be attributed to the presence of oxygen vacancy state between the valence band and conduction band due to the formation of Ti<sup>3+</sup> in the system of carbon-doped TiO<sub>2</sub> (Xiao et al., 2008), or by narrowing the band gap or formed intra-gap localized level (Li et al., 2008). Even though excellent results can be achieved by applying this modification method, high consumption of energy is required due to the calcination process or heating treatment under specific conditions (Kosowska et al., 2005).

### **1.7.5 Utilizing different heterojunction systems**

Heterojunction system means the coupling aspect of two different semiconductors such as CdS/TiO<sub>2</sub> and/or Bi<sub>2</sub>S<sub>3</sub>/TiO<sub>2</sub>. Both heterojunction systems were prepared by two different methods, which are, either direct mixing of these semiconductors or by precipitation of one semiconductor which acts as sensitizer over the other semiconductor which acts as supported material. Thus, utilizing two semiconductors in contact with each other in different redox energy levels of their corresponding conduction bands and valence bands can improve separation process of electron-hole pair. This prolongs the life times of the charge carriers and as a result improves the efficiency of the interfacial charge to the adsorbed pollutants on the heterojunction system surface. However, the photocatalytic efficiency of the heterojunction system strongly depends on the preparation method, how good is the surface contact between the two semiconductors and the type of the treated substrate (Bessekhouad et al., 2004).

### **1.7.6 Utilization of thin films**

Utilizing a fixed TiO<sub>2</sub> photocatalyst has very important operational advantages such as the time saved and photocatalyst material by eliminating the need of catalyst powder recovery during the photocatalytic process. However, the overall photocatalytic performance of the fixed TiO<sub>2</sub> thin films decrease compared to the corresponding slurry mode of the TiO<sub>2</sub> powder. Since the photocatalytic process is a surface phenomenon rather than volume or mass phenomenon (Damodar and Swaminathan, 2008), easy access to the light irradiation and organic pollutants is fundamental for the effective photocatalytic degradation. Thus, fixed TiO<sub>2</sub> thin film